The inner craniodental anatomy of the *Papio* specimen U.W. 88-886 from the Early Pleistocene site of Malapa, Gauteng, South Africa

Florian Bouchet[1*], Alexandre Ribéron[1], Jason L. Heaton[2,3,4§], Jakobus Hoffman[5], Lunga Bam[5], Kudakwashe Jakata[2], Mirriam Tawane[6], Christophe Tenailleau[7], Bernhard Zipfel[2] & Amélie Beaudet[8,9]

[1]*Laboratoire Évolution et Diversité Biologique, Université Toulouse 3 Paul Sabatier, 118 Route de Narbonne, UMR 5174, 31062, Toulouse, France*

[2]*Evolutionary Studies Institute, University of the Witwatersrand, 1 Jan Smuts Avenue, Braamfontein, Johannesburg, 2000 South Africa*

[3]*Department of Biology, Birmingham-Southern College, 900 Arkadelphia Road, AL 35254, Birmingham, USA*

[4]*Plio-Pleistocene Palaeontology Section, Department of Vertebrates, Ditsong National Museum of Natural History, 432 Paul Kruger Street, Pretoria, Pretoria, 0001 South Africa*

[5]*South African Nuclear Energy Corporation SOC Ltd. (Necsa), R104 Pelindaba, Elias Motsoaledi Street Extension (Church Street West), Hartbeespoort, Madibeng Municipality, 0240 South Africa*

[6]*Ditsong National Museum of Natural History, 432 Paul Kruger Street, Pretoria, Pretoria, 0001 South Africa*

[7]*Centre Inter-universitaire de Recherche et d'Ingénierie des Matériaux (CIRIMAT), Université Toulouse 3 Paul Sabatier, 118 Route de Narbonne, UMR 5085 CNRS-INP-UPS, 31062, Toulouse, France*

[8]*School of Geography, Archaeology and Environmental Studies, University of the Witwatersrand, 1 Jan Smuts Avenue, Braamfontein, Johannesburg, 2000 South Africa*

[9]*Department of Anatomy, University of Pretoria, Lynnwood Road, Hatfield, Pretoria, 0002 South Africa*

Received 17 October 2018. Accepted 15 February 2019

Cercopithecoids represent an essential component of the Plio-Pleistocene faunal assemblage. However, despite the abundance of the cercopithecoid fossil remains in African Plio-Pleistocene deposits, the chronological and geographic contexts from which the modern baboons (i.e. *Papio hamadryas* ssp.) emerged are still debated. The recently discovered *Papio* (*hamadryas*) *angusticeps* specimen (U.W. 88-886) from the *Australopithecus sediba*-bearing site of Malapa, Gauteng, South Africa, may represent the first modern baboon occurrence in the fossil record. Given the implication of U.W. 88-886 for the understanding of the papionin evolutionary history and the potential of internal craniodental structures for exploring evolutionary trends in fossil monkey taxa, we use X-ray microtomography to investigate the inner craniodental anatomy of this critical specimen. Our goal is to provide additional evidence to examine the origins of modern baboons. In particular, we explore (i) the tissue proportions and the dentine topographic distribution in dental roots and (ii) the endocranial organization. Consistent with the previous description and metrical analyses of its external cranial morphology, U.W. 88-886 shares internal craniodental anatomy similarities with Plio-Pleistocene and modern *Papio*, supporting its attribution to *Papio* (*hamadryas*) *angusticeps*. Interestingly, average dentine thickness and distribution in U.W. 88-886 fit more closely to the extinct *Papio* condition, while the sulcal pattern and relative dentine thickness are more like the extant *Papio* states. Besides providing additional evidence for characterizing South African fossil papionins, our study sheds new light on the polarity of inner craniodental features in the papionin lineage.

Keywords: modern baboons, Cradle of Humankind, papionins, endocast, tooth roots.

INTRODUCTION

Cercopithecoids, or Old World monkeys, represent the most successful lineage among nonhuman primates in terms of both demographic and geographic expansion (Frost *et al*. 2011; Elton 2006). The papionin clade includes the medium-to-large bodied species of this highly diverse family, such as the extant baboons (*Papio*), geladas (*Theropithecus*), macaques (*Macaca*), mandrills and drills (*Mandrillus*), and mangabeys (*Cercocebus*, *Lophocebus*). The recently discovered 'Kipunji monkey' (genus *Rungwecebus*, Davenport *et al*. 2006) may also represent an additional papionin taxon phylogenetically related either to *Papio* or to *Lophocebus*, based respectively on DNA and morphological analyses (Davenport *et al*. 2006; Zinner *et al*. 2009; Singleton *et al*. 2010; Gilbert *et al*. 2011). The African primate fossil record reveals a critical adaptive radiation in the papionin lineage during the Plio-Pleisto-

*Author for correspondence. E-mail: bouchet.florian0@orange.fr

cene (Delson 1975; Fleagle 2013). In particular, the South African fossil monkey assemblages document the presence of up to 10 fossil papionin species, including extinct (i.e. *Dinopithecus*, *Gorgopithecus*, *Parapapio*) and extant (i.e. *Papio*, *Theropithecus*) genera (Freedman 1957; Szalay & Delson 1979; Delson 1984, 1988; Jablonski 2002; Gilbert 2007; Williams *et al*. 2007; Jablonski & Frost 2010; Gilbert 2013).

However, despite the relative abundance of the African papionin fossil remains, debates on papionin alpha taxonomy questioning the validity of historical (e.g. *Parapapio*) and newly erected (e.g. *Procercocebus antiquus*, *Soromandrillus quadratirostris)* species prevent further clarification of their evolutionary history (Heaton 2006; Gilbert 2007; Jablonski & Frost 2010; Gilbert 2013). While recent refinements of papionin phylogeny have combined both molecular and morphological evidence (e.g. Gilbert 2007; Gilbert & Rossie 2007; Gilbert *et al*. 2009), the phylogenetic relationships between the papionin clades, in particular *Lophocebus*, *Papio*, *Rungwecebus* and *Theropithecus*, are still debated or simply unknown (Gilbert *et al*. 2011; Gilbert 2013; Gilbert *et al*. 2018). These uncertainties complicate evolutionary reconstructions such as that of the *Papio* lineage and its modern representatives (i.e. *Papio hamadryas* ssp.), for which chronological and geographic origins are largely questioned.

Molecular analyses performed on living populations estimated the origin and radiation of modern *Papio hamadryas* to be between 1.8 and 2.2 Ma in South Africa (Newman *et al*. 2004; Zinner *et al*. 2013). To date, fossil remains of early modern baboons have been described in East African (Alemseged 2000; Frost 2007; Frost & Alemseged 2007) and South African Middle Pleistocene deposits (Freedman 1957; Jablonski 2002; Williams *et al*. 2012). More specifically, because of substantial synapomorphies shared with extant *Papio hamadryas* subspecies, the *Papio angusticeps* specimens found in Cooper's Cave, Gladysvale and Kromdraai, have been suggested to represent a subspecies of modern baboon (Delson 1988; Gilbert 2013; Gilbert *et al*. 2018). Unfortunately, notwithstanding previous valuable applications of relative dating (e.g. Steininger *et al*. 2008; Herries *et al*. 2009; Pickford 2013), the geological ages of these three sites remain uncertain (see Bruxelles *et al*. 2016 for discussion and perspectives at Kromdraai).

In this context, the papionin specimen U.W. 88-886 found in the early Pleistocene deposits of the *Australopithecus sediba*-bearing site of Malapa and attributed to a male *Papio angusticeps* specimen by Gilbert *et al*. (2015) has the potential to shed new light on the emergence of modern baboons (Berger *et al*. 2010). Indeed, the application of absolute and relative dating methods provided an age of ~2.026–2.36 Ma. Therefore, U.W. 88-886 may represent the earliest fossil evidence of *Papio angusticeps* and consequently, of the modern baboon, in a calibrated chronological context (Gilbert *et al*. 2015).

Given the implication of U.W. 88-886 for understanding *Papio* evolutionary history and the potential of inner craniodental structures for exploring the evolutionary trends among fossil monkey taxa (e.g. Beaudet *et al*. 2015, 2016a–c), we have chosen to use micro-focus X-ray tomography to investigate the inner craniodental anatomy of this critical specimen.

Inner craniodental structures have demonstrated relevance for discussing primate taxonomy and phylogeny. More specifically, dental root tissue proportions (Kupczik & Hublin 2010; Le Cabec *et al*. 2012, 2013) and distribution of the radicular dentine (Bondioli *et al*. 2010; Bayle *et al*. 2011; Macchiarelli *et al*. 2013; Zanolli *et al*. 2014) are particularly informative for distinguishing closely related taxa. Moreover, previous descriptions of cerebral imprints on fossil primate endocasts have revealed the potential of sulci for clarifying the taxonomic or phylogenetic contexts of fossil taxa (e.g. Connolly 1953; Radinsky 1974; Falk 1981; Gonzales *et al*. 2015; Beaudet *et al*. 2016c). Such considerations show the potential of inner dental root features and sulcal pattern for distinguishing between taxa of very low taxonomic ranks, as it is the case for baboons. Additionally, studies of meningeal artery imprints in primate fossil endocasts and extant brains suggest a shift in the source of the cerebral blood supply during the course of primate evolution relating potentially to a phylogenetic effect (Falk 1993; Bruner & Sherkhat 2008; de Lázaro *et al*. 2018). On the other hand, inner craniodental structures appear to hold information linked to the biology of the organisms. Root morphology may be related to biomechanics and diet (Spencer 2003; Kupczik *et al*. 2009) whereas sulcal pattern may have functional implications (Falk 1978, 1981).

Due to the peculiar status of U.W. 88-886 as the first possible occurrence of modern baboons, we aim at furthering our view of the paleobiology and potential adaptations in *Papio* and papionins in general. Another objective of this study is to discuss the polarity of inner craniodental features in these lineages.

Because of its potential for providing taxonomic and especially phylogenetic and biological-related information, we investigate the inner craniodental anatomy of U.W.88-886 and provide additional evidence to discuss both the origins and diversity of modern baboons, as well as papionin evolutionary history. Here we explore: (i) the tissue proportions and topographic distribution of dentine in the distobuccal root of the right upper third molar (UM3) and (ii) the sulcal and vascular imprints from the endocranial surface. We hypothesize that the internal craniodental morphology in U.W. 88-886 will be intermediate between the Plio-Pleistocene *Papio* species, such as *Papio izodi* and *Papio robinsoni*, and modern *Papio hamadryas* taxa. Evolution of the brain and posterior teeth have been shown to be decoupled in several Plio-Pleistocene hominins (Gómez-Robles *et al*. 2017). Previous studies have shown that all species within *Papio* had similar molar size except *Papio izodi* which exhibited larger molars relative to overall cranial size (e.g. Freedman 1957; Gilbert *et al*. 2015, 2018). Thus, although subsequent *Papio* taxa have not undergone evolutionary changes in terms of relative molar size, an apparent molar reduction occurred when *Papio* began to diverge. On the contrary, studies dealing with endocranial volume suggested that there were no significant temporal changes in cercopithecoid brain size

(e.g. Elton 2001; Beaudet *et al*. 2016c). Therefore, the *Papio* genus may have never experienced brain size changes throughout its evolution. Based on these findings we may expect to identify differences in terms of key evolutionary signals in the endocast and roots.

MATERIALS AND METHODS

Comparative sample

Our fossil comparative sample consists of 7 extinct papionin taxa selected from different stratigraphic units of the Plio-Pleistocene sites of Kromdraai, Makapansgat, Sterkfontein, Swartkrans and Taung (South Africa; Table 1). Mindful of ongoing debates on papionin alpha taxonomy (e.g. Delson 1988; Heaton 2006; Gilbert 2007; Williams *et al*. 2007; Jablonski & Frost 2010; Gilbert 2013; Gilbert *et al*. 2013), here we follow the most consensual nomenclature (notably used in Beaudet *et al*. 2016b,c).

Our comparative sample includes 22 specimens representing six extant genera (Table 1). All specimens considered in this study are fully mature and we systematically checked the degree of apical closure in the specimens used for assessing dental features. Because we focus on adult roots and endocasts, we preferentially chose specimens with apically closed UM3 and good preservation of the endocranium.

Scanning protocol

In January 2018, the U.W. 88-886 specimen was detailed by X-ray microtomography (μCT) at the Palaeosciences Centre of the Evolutionary Studies Institute (University of the Witwatersrand, Johannesburg, South Africa). The acquisitions were performed by using a Nikon Metrology XTH 225/320 LC dual source μCT scanner with the following parameters: 155 μA current, 90 kV voltage and 1 s exposition time per projection. The final reconstructed volume has a voxel size of 44.43 × 44.43 × 44.43 μm. All specimens investigated in this study have been similarly imaged by μCT through various systems with a spatial resolution ranging from 33 to 129.63 ìm (Table 1).

The sample size of the dental tissue proportions investigated, plus endocasts explored, are listed in Table 1.

Upper third molar virtual reconstruction and dental tissue proportions and distribution

As previously reported by Gilbert *et al*. (2015, see Fig. 2) and based upon external visual inspection of U.W. 88-886, the specimen only preserves the roots of the upper second (UM2) and third molars (UM3). In fact, our microtomographic-based investigation of the specimen reveals that the UM3 roots are well-preserved (Fig. 1A,B). We virtually reconstructed the UM3 roots by using a semi-automatic threshold-based segmentation and mesh reconstruction via Avizo Lite v9.0.1 (Visualization Sciences Group Inc.). We focused our measurements on the complete distobuccal root (Fig. 1E,F). Accordingly, we virtually separated the distobuccal root by using a 3D plane passing through three landmarks positioned on the three radicular apices (Fig. 1C). This plane has been translated towards the furcation of the three roots until the distobuccal and lingual roots are fused and used as a cutting plane to separate the distobuccal root from the rest of the tooth (Fig. 1D).

In all specimens, the following variables describing tissue proportions and structural organization were assessed (Avizo v9.0.1): surface of the dentine–enamel junction (SDPJ, mm^2), volume of the dentine (V_d, mm^3), volume of the pulp (V_p, mm^3) and total volume (V_t, mm^3). Based on these values we calculated three indices: the percent of volume that is pulp (V_p/V_t, %), the 3D average dentine thickness (3D ADT = V_d/SDPJ, mm) and the scale-free 3D relative dentine thickness (3D RDT = 100*3D ADT/[$V_p^{1/3}$]) (Kono 2004; Olejniczak *et al*. 2008a,b, Beaudet *et al*. 2015, 2016a,b, Zanolli *et al*. 2018).

The topographic distribution of the dentine was virtually rendered by computing the distances between the dentine and pulp surfaces ('Surface Distance' module on Avizo v9.0.1). The distances recorded were visualized at the outer dentine surface using a colour scale ranging from dark blue ('thinner') to red ('thicker') (Bayle *et al*. 2011).

Endocast reconstruction and automatic detection of the sulcal and vascular patterns

The endocast of U.W. 88-886 has been virtually reconstructed by removing the sediment from the inner surface of the cranium using semi-automatic threshold-based segmentation (Avizo Lite v9.0.1) and subsequently applying automatic segmentation through the Endex software on the remaining cranial bones (Subsol *et al*. 2010; http://liris.cnrs.fr/gillesgesquiere/wiki/doku.php?id¼endex).

We used an automatic method to identify the crests and ravines on the endocast surfaces which correspond respectively to the meningeal arteries and sulci (see Beaudet *et al*. 2016c for further details). The detected structures were corrected manually by removing non-anatomical features (e.g. cracks due to taphonomic damage) using published studies of cercopithecoid endocasts as references (Connolly 1950; Castelli & Huelke 1965; Falk 1978, 1981; Falk & Nicholls 1992; Beaudet *et al*. 2016c). This 'cleaning' step was performed using a program created with MATLAB R2013a v8.1 (Mathworks) (Beaudet *et al*. 2016c).

RESULTS

Tissue proportions and distribution in the distobuccal root

Values of tissue proportions of the UM3 distobuccal root in U.W. 88-886 and in the comparative papionin sample are shown in Table 2. The absolute volumes of dentine and pulp, the total root volume and the surface area of the dentine–pulp junction in U.W. 88-886 are higher than in extant *Cercocebus*, *Lophocebus*, *Macaca* and *Theropithecus* specimens and globally lower than in extant *Papio* and *Mandrillus* as well as in extinct *Papio*, *Parapapio* and *Theropithecus* specimens (Table 2). By considering all the absolute variables reported in Table 2, to the exception of the pulp volume (i.e. V_d, V_t, SPDJ), U.W. 88-886 is closer to extant *Theropithecus* than to any other taxa (Table 2). In terms of proportions, the dentine represents 95.57% of the

Table 1. List of the Plio-Pleistocene and extant papionin specimens/samples detailed by X-ray microtomography (μCT) and used for assessing tooth tissue proportions and endocranial organization as compared to U.W. 88-886.

(**A**) Specimen/sample			Site/provenance	References	Stored at	μCT equipment	μCT acquisition voxel size (μm)	Elements	
								UM3[a] distobuccal root	Endocast
Fossil taxa									
U.W. 88-886			Malapa	Gilbert *et al*. 2015.	Wits[b]	Pal. Centre[1]	44.43	1	1
Papio angusticeps	*n* = 1	KA 194	Kromdraai A	Freedman 1957; Brain 1981.	Ditsong[c]	Necsa[2]	74	1	_
Papio izodi	*n* = 1	TP 4	Taung	Freedman 1957, 1961.	Wits[b]	Pal. Centre[1]	79	1	_
Papio robinsoni	*n* = 2	SK 555, SK 562	Swartkrans (Member 1)	Freedman 1957; Brain 1981; Jablonski 2002.	Distong[b]	Necsa[2]	57–78	2	_
Parapapio antiquus	*n* = 1	TP 8	Taung	Freedman 1957, 1961.	Wits[b]	Pal. Centre[1]	80	_	1
Parapapio broomi	*n* = 2	STS 544, STS 564	Sterkfontein (Member 4)	Freedman 1957; Eisenhart 1974; Brain 1981; Heaton 2006.	Ditsong[c]	Necsa[2]	50–72	1	1
Parapapapio whitei	*n* = 1	MP 221	Makapansgat (Member 4?)	Freedman 1976; Gilbert 2013.	Wits[b]	Pal. Centre[1]	71	1	1
Theropithecus oswaldi darti	*n* = 2	M 3073, MP 222	Makapansgat (Member 4)	Maier 1972; Freedman 1976; Jablonski 1993, 2002; Jablonski & Frost 2010.	Wits[b]	Pal. Centre[1]	71	1	2

(**B**) Specimen/sample		Site/provenance	Stored at	μCT equipment	μCT acquisition voxel size (μm)	Elements	
						UM3 distobuccal root	Endocranial organization
Extant taxa							
Cercocebus, (*agilis n* = 2 *atys n* = 1, *torquatus n* = 1)	*n* = 4	Cameroon, Dem. Rep. Congo, Liberia.	AMNH[d], MRAC[e]	FERMaT[3], MIF[4]	33–68.15	2	2
Lophocebus (*albigena n* = 2, *johnstoni n* = 2)	*n* = 4	Cameroon, Dem. Rep. Congo, Gabon.	AMNH[d], MNHN[f], MRAC[e]	AST-RX[5], FERMaT[3], MIF[4]	33-91.92	2	2
Macaca (*mulatta n* = 1, *Sylvanus n* = 3)	*n* = 4	India, unknown provenance.	AMNH[d], MHNT[g]	FERMaT[3], MIF[4]	33–129.63	2	2
Mandrillus (*leucophaeus n* = 2, *sphinx n* = 2)	*n* = 4	Cameroon, unknown provenance.	AMNH[d], MRAC[e]	FERMaT[3], MIF[4]	33–84.15	2	2
Papio (*anubis n* = 3, *hamadryas n* = 1)	*n* = 4	Cent. Af. Rep., Dem. Rep. Congo, Ethiopia.	AMNH[d], MNHN[f]	AST-RX[5], MIF[4]	55-123	2	2
Theropithecus (*gelada n* = 2)	*n* = 2	Ethiopia.	MNHN[f]	AST-RX[5]	76–96	2	2

[a]UM3: upper third molar. [b]University of the Witwatersrand, Johannesburg; [c]Ditsong National Museum of Natural History, Pretoria; [d]American Museum of Natural History, New York; [e]Musée royal de l'Afrique centrale, Tervuren; [f]Muséum national d'Histoire naturelle, Paris; [g]Muséum d'Histoire naturelle de Toulouse. [1]Palaeosciences Centre, University of the Witwatersrand, Johannesburg; [2]South African Nuclear Energy Corporation, Pretoria (Hoffman & de Beer, 2012); [3]Fluides Energie Réacteurs Matériaux et Transferts, Toulouse; [4]Microscopy and Imaging Facility, AMNH, New York (data provided by Pr Eric Delson and the AMNH Department of Mammalogy, some specimens were downloaded from www.morphosource.org, Duke University); [5]Accès Scientifique à la Tomographie à Rayons-X, MNHN, Paris.

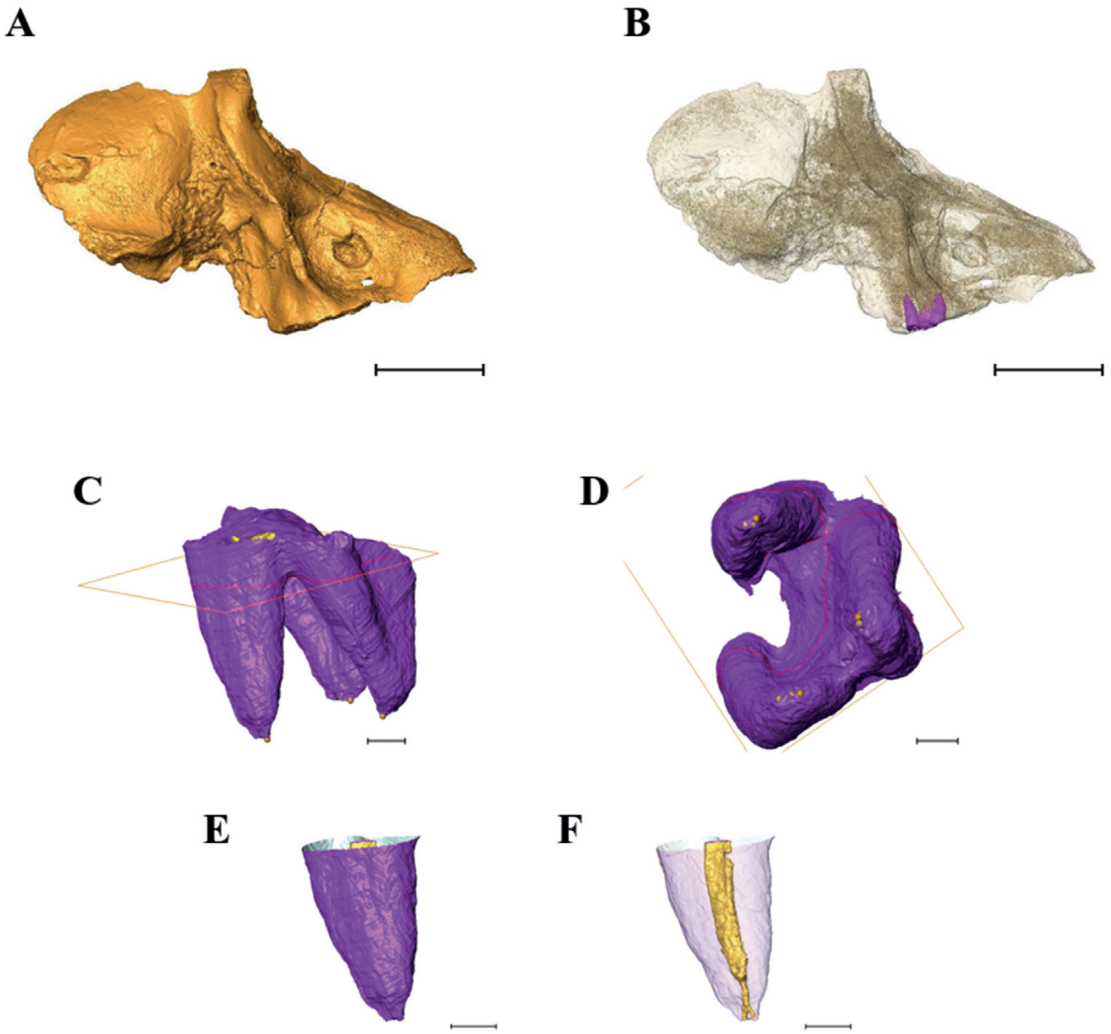

Figure 1. **A**, virtual rendering of U.W. 88-886 in lateral view and **B**, in semi-transparency showing the roots of the upper third molar. **C**, the cutting plane separating the distobuccal root is parallel to the landmarks placed on the three radicular apices and **D**, is positioned where the distobuccal and lingual roots are fused. **E**, virtual rendering of the distobuccal root and **F**, of the pulp (in yellow) and dentine (in purple). Scale bars equal: A, B, 3 cm; C–F, 2 mm.

total volume of the root in U.W. 88-886, which closely fits the range of values found in the extant *Lophocebus* (93.05–98.05%, Table 2, Fig. 2A,B) and *Mandrillus* (94.47–97.23%, Table 2, Fig. 2A,B) specimens.

Considering the dentine thickness, the ADT (2.76 mm) and RDT (187.88) in U.W. 88-886 approximate the values reported for extinct (2.86 mm) and extant *Papio* (187.69) respectively, and for extant *Theropithecus* (Table 2, Fig. 2C,D).

Cartographies of dentine thickness topographical variation are rendered on the outer distobuccal surface of U.W. 88-886 and comparative papionin specimens in Figs 3 and 4. We used an individual scale ranging from the minimum to the maximal value for each specimen. In U.W. 88-886, the dentine is moderately thick along the distobuccal root with the thickest areas located at the most superior mesiobuccal aspect (Fig. 3). This pattern fits the condition of the two fossil *Papio* specimens (i.e. KA 194 and SK 562) and, to a lesser extent, of extant *Cercocebus* and *Theropithecus* (Figs 3 and 4).

Structural organization of the endocast

The endocast of U.W. 88-886 consists mainly of the portion of the temporal lobe posterior to the temporal pole and inferior to the frontal lobe, the inferior portion of the posterior frontal part and the most inferior part of the parietal lobe. Detected structures are shown in Fig. 5. The sulcal patterns detected and identified in the comparative papionin specimens are shown in Figs 6 and 7.

In the inferior part of the temporal lobe, we detected the imprints of two sulci (S1 and S2, Fig. 5) and two arteries (V1 and V2, Fig. 5). S1 is deep and seems to be continuous in the ventral border of the temporal lobe (Fig. 5B). S2 runs superiorly to S1 (Fig. 5A). V1 is found between the two sulci S1 and S2 while V2 is located in the inferior part of the temporal lobe (Fig. 5).

Based on primate brain atlases and respective location and connection of the sulci, S1 and S2 can be tentatively identified as the occipito-temporal sulcus and a posterior segment of the middle temporal sulcus (hereafter named 'posterior middle temporal sulcus'), respectively (Fig. 6). Concerning V1 and V2, based on the previous descriptions of meningeal arteries in extant macaques (e.g. Castelli & Huelke 1965; Falk & Nicholls 1992), we suggest that they correspond to the anterior and posterior branches of the middle meningeal artery (main branch) (Fig. 6), respectively.

A faint depression was detected in the superior part of

Table 2. 3D distobuccal root tissue proportions of the upper third molar in U.W. 88-886 and in some Plio-Pleistocene and extant papionin specimens/samples.

Specimen/sample			V_d (mm^3)	V_p (mm^3)	V_t (mm^3)	SDPJ (mm^2)	V_p/V_t (%)	3D ADT (mm)	3D RDT
U.W. 88-886			68.41	3.17	71.58	24.78	4.43	2.76	187.88
Fossil taxa									
Papio	*angusticeps*	KA 194	48	10.99	58.99	13.18	18.63	3.64	163.72
	izodi	TP 4	43.78	1.55	45.33	14.47	3.42	3.03	261.82
	robinsoni	SK 555	153.96	17.75	171.71	63.74	10.34	2.42	92.77
	robinsoni	SK 562	96.95	9.94	106.89	41.49	9.30	2.34	108.83
		Mean	85.67	10.06	95.73	33.22	10.42	2.86	156.78
Parapapio	*broomi*	STS 544	70.72	4.58	75.30	27.56	6.08	2.57	154.75
	whitei	MP 221	86.34	10.85	97.19	45.34	11.16	1.90	85.82
		Mean	78.53	7.71	86.25	36.45	8.62	2.23	120.28
Theropithecus	*oswaldi darti*	MP 222	174.53	7.28	181.81	37.67	4.00	4.63	238.89
Extant taxa									
Cercocebus		Mean	19.06	0.62	19.69	9.62	3.08	2.13	264.26
		Range (n = 2)	13.29–24.84	0.38–0.87	13.67–25.71	5.38–13.87	2.78–3.38	1.79–2.47	187.51–341.01
Lophocebus		Mean	21.03	0.99	22.02	9.23	4.45	2.56	300.96
		Range (n = 2)	21.16–20.90	0.42–1.56	21.58–22.46	6.20–12.27	1.95–6.95	1.70–3.41	146.58–455.34
Macaca		Mean	36.10	0.99	37.09	12.77	2.59	2.85	298.33
		Range (n = 2)	24.69–47.51	0.59–1.40	25.28–48.91	8.45–17.09	2.33–2.86	2.78–2.92	248.51–348.15
Mandrillus		Mean	76.90	3.92	80.82	31.36	4.15	2.87	229.04
		Range (n = 2)	38.55–115.25	1.10–6.74	39.65–121.99	10.98–51.74	2.77–5.53	2.23–3.51	118.06–340.02
Papio		Mean	117.11	7.34	124.45	33.24	5.89	3.58	187.69
		Range (n = 2)	115.88–118.35	5.84–8.83	124.19–124.71	29.20–37.28	4.70–7.08	3.11–4.05	150.47–224.09
Theropithecus		Mean	63.45	5.25	68.69	26.62	7.14	2.66	182.94
		Range (n = 2)	57.94–68.95	1.95–8.55	59.89–77.50	16.98–36.27	3.26–11.03	1.90–3.41	92.92–272.95

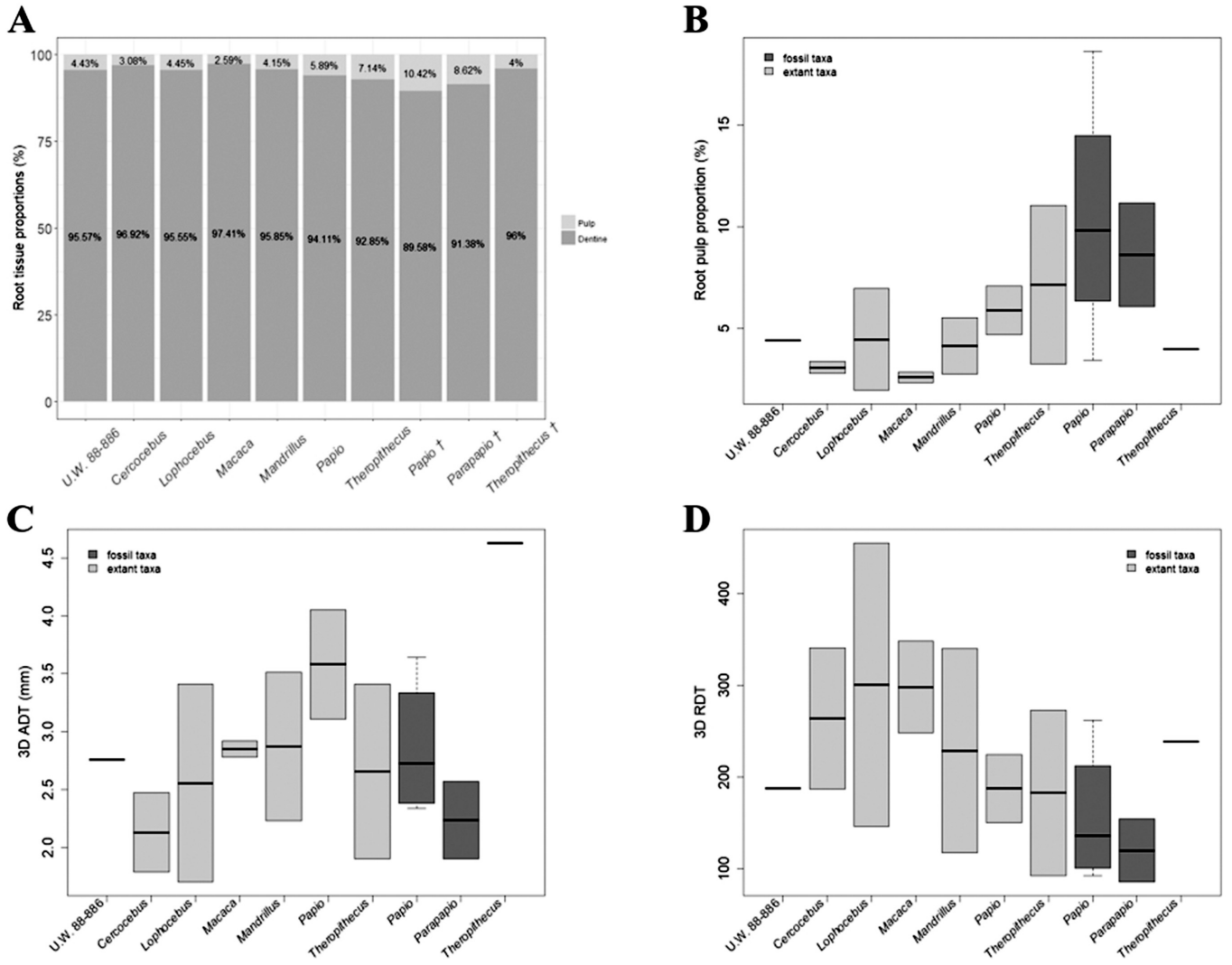

Figure 2. 3D distobuccal root tissue proportions of the upper third molar in U.W. 88-886 and in some Plio-Pleistocene and extant papionin specimens/samples. **A**, barplot of the tissue proportions in the distobuccal root. **B**, boxplot of the percentage of pulp in the distobuccal root (V_p/V_t). **C**, boxplot of the 3D average dentine thickness in the distobuccal root (3D AET). **D**, boxplot of the 3D relative dentine thickness in the distobuccal root (3D RDT).

the temporal lobe of U.W. 88-886 (S3, Fig. 5A) that could be identified as the Sylvian fissure (Fig. 6). This depression runs along a thick artery (V3, Fig. 5A), which is part of the anterior meningeal artery branching.

In the frontal lobe, we detected two sulci posterior (S4, Fig. 5A) and anterior (S5, Fig. 5A) to a cluster of terminal arteries (V4, Fig. 5A). The respective location of S4 and S5 is compatible with an attribution to the anterior subcentral sulcus and the inferior branch of the arcuate sulcus, respectively (Fig. 6). V3 and the cluster of arteries labelled V4 in U.W. 88-866 probably correspond to the anterior meningeal artery and its ramifications.

When compared to fossil and extant papionins, the sulcal pattern in U.W. 88-886 approximates that of extant *Theropithecus* and extant *Papio* specimens (Fig. 7). Indeed, the endocasts in these two genera show the anterior subcentral, occipito-temporal (lateral) and posterior middle temporal sulci (Fig. 7), as in U.W. 88-886 (Fig. 6). The meningeal artery pattern described in U.W. 88-886 is compatible with the 'pattern A' described by Falk & Nicholls (1992, see Fig. 2A) which might point out that the most common pattern originally present in macaques has been retained during papionin evolution.

DISCUSSION

In terms of tissue proportion and distribution and of cerebral organization, U.W. 88-886 shares similarities with extinct and extant *Papio* specimens. Accordingly, our study suggests that, in terms of inner craniodental anatomy, U.W. 88-886 possesses a combination of derived (i.e. extant *Papio*-like) and primitive (i.e. extinct *Papio*-like) features. These results support both the previous attribution of U.W. 88-886 to *Papio* (*hamadryas*) *angusticeps* and a basal phylogenetic position of this taxon among modern baboons (Gilbert *et al*. 2015; Gilbert *et al*. 2018). In this context, our results provide evidence for discussing the tempo and mode of the evolution of craniodental features in papionins. Based on the dating of the U.W. 88-886-bearing layer in Malapa, our analyses may indicate that the modern relative root dentine thickness and cerebral organization emerged early within the *Papio* lineage (i.e. ~2.36 Ma), while other dental aspects, such as the average root dentine thickness and dentine distribution, could have developed after approximately 2 Ma. Accordingly, our results may suggest a mosaic evolution of craniodental traits in the papionin lineage. Recently, *Papio hamadryas anubis* has been suggested to retain ancestral

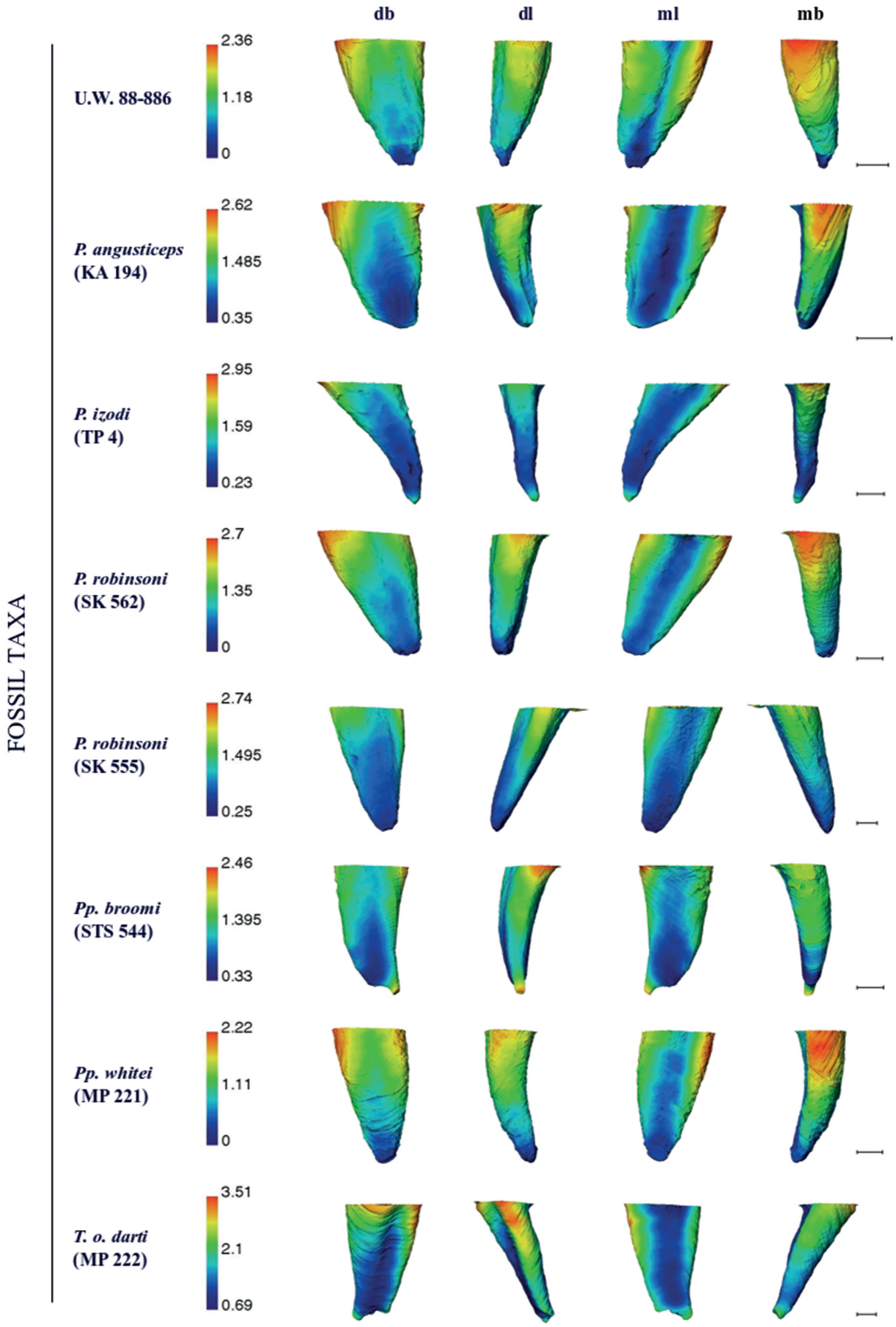

Figure 3. Dentine thickness cartographies of the UM3 distobuccal root in U.W. 88-886 and in some Plio-Pleistocene papionin specimens. Topographic thickness variation is rendered by a pseudo-colour scale ranging from thinner dark-blue to thicker red. Independently from their original side, all roots are shown as right and imaged in distobuccal (db), distolingual (dl), mesiolingual (ml) and mesiobuccal (mb) views. Because of significant variation in dentine thickness between species, a specific colour scale is attributed to each specimen (in mm). Scale bars equal: 2 mm.

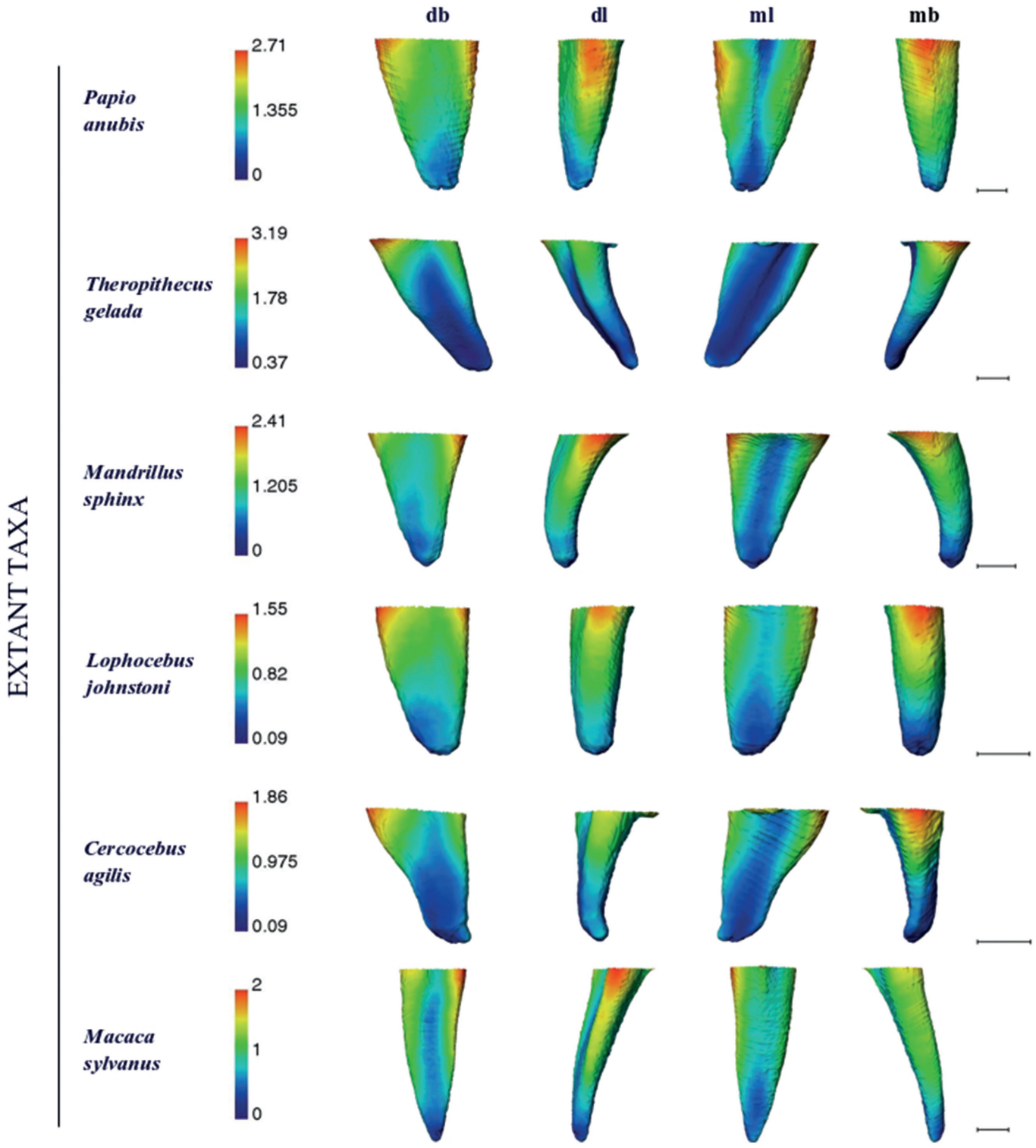

Figure 4. Dentine thickness cartographies of the UM3 distobuccal root of some selected extant papionin specimens. Topographic thickness variation is rendered by a pseudo-colour scale ranging from thinner dark-blue to thicker red. Independently from their original side, all roots are shown as right and imaged in distobuccal (db), distolingual (dl), mesiolingual (ml) and mesiobuccal (mb) views. Because of significant variation in dentine thickness between species, a specific colour scale is attributed to each specimen (in mm). Scale bars equal: 2 mm.

Papio robinsoni-like external craniodental features (Gilbert *et al*. 2018). Based upon inner dental variables considered here, our results demonstrate that *Papio hamadryas anubis* is more similar to U.W. 88-886 than to any other Plio-Pleistocene *Papio* specimens/taxa. However, given that our dental sample of *Papio hamadryas anubis* is limited to two specimens, dental variation in this taxa might not be representative here. Further studies are required to fully assess the polarity of craniodental characters, especially those related to inner craniodental structures.

Additionally, in a broader taxonomic context/perspective, our results point to similarities in terms of average and relative dentine thickness between extinct and extant *Papio* specimens, including U.W. 88-886, and extant *Theropithecus*. Interestingly, tissue proportions in the UM3 crown, and more particularly the average and relative

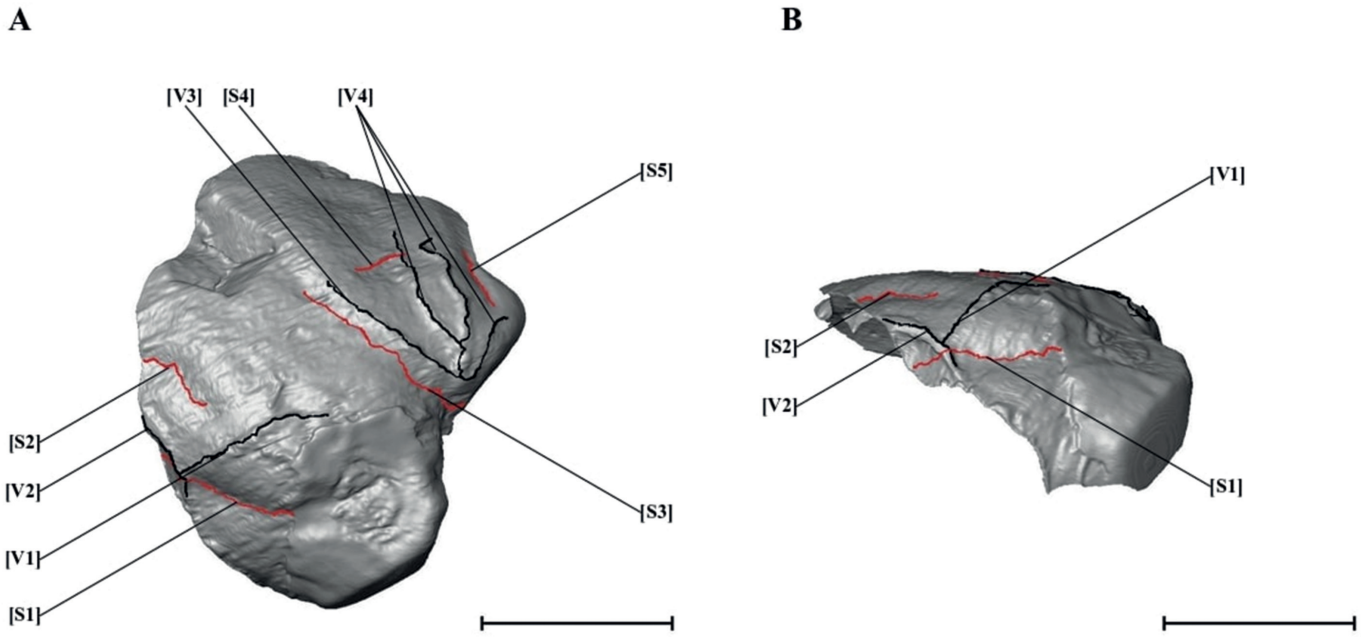

Figure 5. **A**, virtual reconstruction of U.W. 88-886 with sulcal and meningeal impressions in lateral right and **B**, inferior views. S: sulcus, V: vessel. Scale bars equal: 2 cm.

enamel thickness, have been previously suggested to be comparable between these taxa, as well (Beaudet *et al*. 2016b).

Because root tissue proportions and morphology have been proven to hold phylogenetic information (Spencer 2003; Kupczik & Hublin 2010; Le Cabec *et al*. 2012, 2013), similarities in the radicular dentine thickness reported in this study could be explained by close phylogenetic relationships. However, previous studies have shown that root morphology may be also related to the distribution of occlusal forces experienced by teeth during feeding (Kovacs 1979; Spencer 1998, 2003; Kupczik *et al*. 2009). In particular, a correlation has been suggested between variation in root morphology and consumption of fallback foods (Kupczik & Dean 2008). Indeed, fallback foods are generally more resistant than preferred foods and thus are expected to be responsive to selective pressures upon dental morphology (Marshall & Wrangham 2007; Kupczik & Dean 2008; Marshall *et al*. 2009). Living baboons are known to be omnivores with a preference for fruits and seeds (e.g. Dunbar & Dunbar 1974; Hamilton *et al*. 1978), but, during the dry season, they rely heavily on underground storage organs (USO, e.g. corms, tubers, roots) as fallback foods (e.g. Hamilton *et al*. 1978; Byrne *et al*. 1993; Altmann 2009). Among Plio-Pleistocene papionins, *Papio robinsoni* from Swartkrans has been proposed to have seasonally incorporated fallback foods illustrating a dietary behaviour similar to living baboons (Codron 2003; El-Zaatari *et al*. 2005). Geladas, on the other hand, are characterized by a highly specialized diet composed of grass blades (e.g. Dunbar & Dunbar 1974; Dunbar 1976; Jarvey *et al*. 2017) but, as baboons do, also consume USO as fallback foods during the dry season (e.g. Fashing *et al*. 2014; Venkataraman *et al*. 2014; Jarvey *et al*. 2017).

Thus, similarities in dentine thickness between geladas, living baboons and Plio-Pleistocene baboons reported in this study could be tentatively explained by convergent adaptations to the consumption of USO. It is likely that the environmental shift that led to more open habitats after 2 Ma in South Africa resulted in the development of various dietary strategies among cercopithecoids (Elton 2012). Habitat reconstructions in Kromdraai A, Swartkrans Member 1 and Sterkfontein Member 5 indicate quite open environments compared to the earlier Member 4 of Sterkfontein reconstructed as a more dense woodland (Vrba 1975; Reed 1997; Bamford 1999). There was turnover of the monkey fauna during this shift (Elton 2007), with *Papio* dispersing northwards from its southern African region of origin (Newman *et al*. 2004; Williams *et al*. 2012; Zinner *et al*. 2013). Further work is needed to explore whether an increased reliance on fallback foods was a factor in *Papio*'s extensive dispersal. From this perspective, U.W. 88-886 may have relied on USO as a fallback food, which is compatible with the Malapa's paleoenvironmental reconstruction (e.g. grassland) between ~1.977 and 2.36 Ma (Kuhn *et al*. 2011).

The study of the topographical variations of the dentine shows that in U.W. 88-886, the thickest areas are located at the most superior mesiobuccal aspect, a pattern that fits to some extent the conditions found for extant *Cercocebus* and *Theropithecus*. Such similarities may be explained either by a durophagous diet all year round in U.W. 88-886 as in *Cercocebus* mangabeys (McGraw *et al*. 2014), or a seasonal consumption of USO as in geladas (Fashing *et al*. 2014). However, the USO consumption hypothesis would be more compatible with the previous discussion on a potential convergent adaptation to the consumption of USO in geladas and *Papio* taxa. Unfortunately, why this thickening of the distobuccal root is absent in extant *Lophocebus* and *Papio* specimens, remains unexplained.

Other craniodental traits such as the presence or

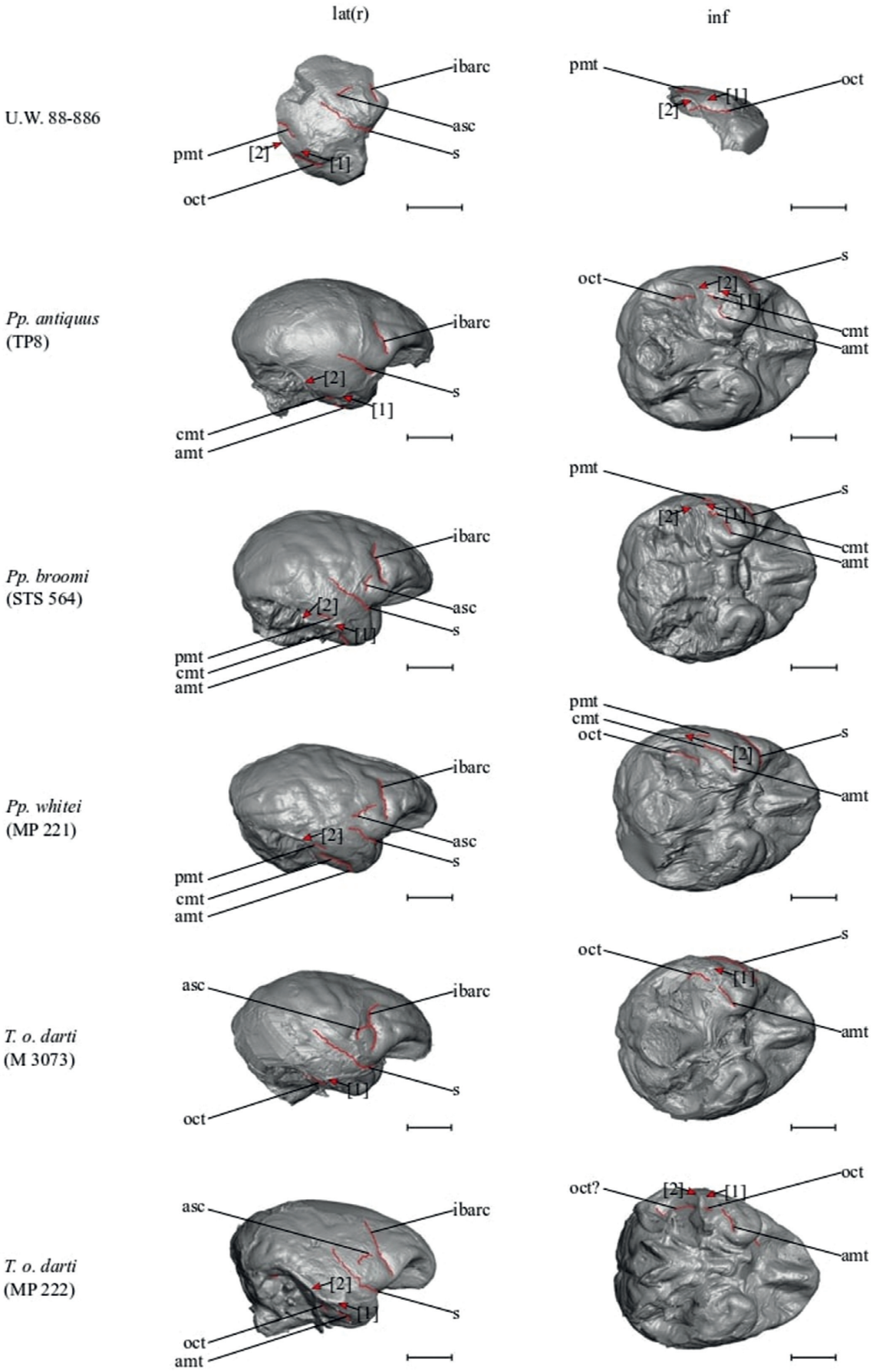

Figure 6. Sulcal impressions in U.W. 88-886 and in some Plio-Pleistocene papionin specimens in lateral (lat) right (r) and inferior (inf) views (amt = anterior middle temporal sulcus, asc = anterior subcentral sulcus, cmt = central middle temporal sulcus, ibarc = inferior branch of the arcuate sulcus, oct = occipito-temporal sulcus, pmt = posterior middle temporal sulcus and s = Sylvian fissure). Only sulci mentioned in the text are labelled. Question marks indicate uncertain sulcal identification. 1: vessel similar to V1 in U.W. 88-886, 2: vessel similar to V2 in U.W. 88-886. Scale bars equal: 2 cm.

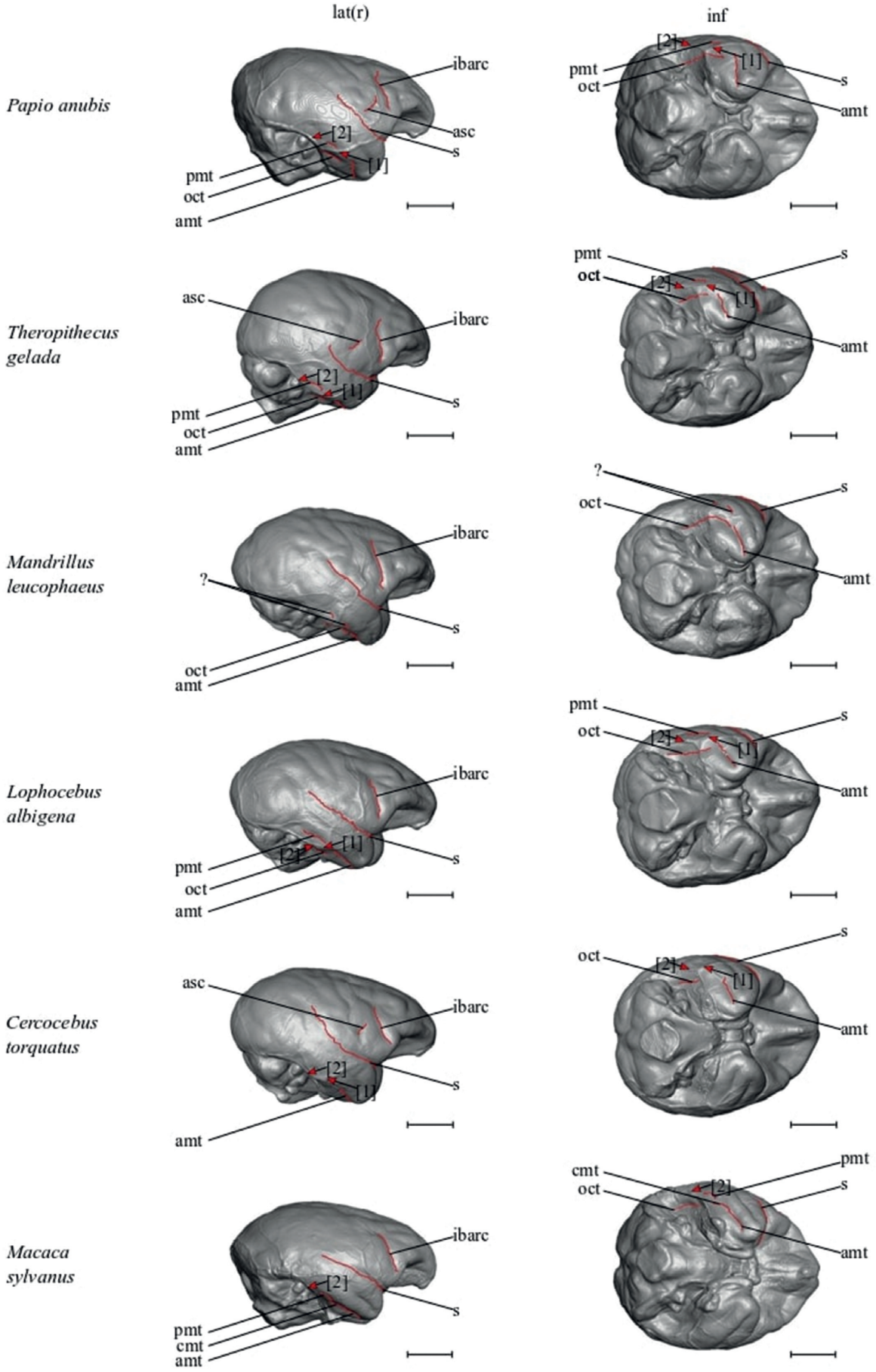

Figure 7. Sulcal impressions in some selected extant papionin specimens in lateral (lat) right (r) and inferior (inf) views (amt = anterior middle temporal sulcus, asc = anterior subcentral sulcus, cmt = central middle temporal sulcus, ibarc = inferior branch of the arcuate sulcus, oct = occipito-temporal sulcus, pmt = posterior middle temporal sulcus and s = Sylvian fissure). Only sulci mentioned in the text are labelled. Question marks indicate uncertain sulcal identification. V1: vessel similar to V1 in U.W. 88-886, V2: vessel similar to V2 in U.W. 88-886. Scale bars equal: 2 cm.

absence of specific endocranial sulci have been demonstrated to provide critical information for discussing the evolutionary history of primate lineages (Connolly 1950; Falk 1978, 1981; Beaudet *et al*. 2016c). In this study, within the limits of our sample, we report high intra- and inter-specific variation in the presence of the anterior subcentral sulcus and the posterior middle temporal sulcus among papionin taxa, notably in *Macaca*. In contrast, we systematically identified the occipito-temporal sulcus (lateral) in all *Cercocebus*, *Lophocebus*, *Mandrillus*, *Papio* and *Theropithecus* specimens considered here. However, this sulcus was absent in the *Macaca* and *Parapapio* endocasts. Accordingly, we can hypothesize that this feature may have been present in the last common ancestor of *Cercocebus*, *Lophocebus*, *Mandrillus*, *Papio* and *Theropithecus* and, should have emerged at about 6.67 Ma (5.37–8.07 Ma, Perelman *et al*. 2011). Furthermore, the absence of this sulcus in *Parapapio* – that is present in crown African papionins – may also support a reconsideration of its position as ancestral to *Papio* which was challenged by recent reconstructions of African papionin phylogenetic relationships (Gilbert 2013; Gilbert *et al*. 2018; Pugh & Gilbert 2018). In this context, in order to test our hypothesis, it may be interesting to explore the sulcal pattern variation in specimens from the oldest South African stratigraphic layers such as the *Papio izodi* and *Parapapio* specimens from Sterkfontein Member 2 (see Heaton 2006) as well as prospective *Parapapio* cranial specimens from the 4–4.5 Ma site of Bolt's Farm (to date BF 43 is the only complete cranium, see Gommery *et al*. 2016).

In *Cercocebus*, *Lophocebus*, *Mandrillus*, *Papio* and *Theropithecus*, the occipito-temporal sulcus is identified on the lateral aspect of the temporal lobe. This configuration has been previously suggested to be specific to the cercopithecines (Falk 1978). However, in our study, the occipito-temporal sulcus (lateral) was absent in *Macaca* and *Parapapio*, which may indicate that this feature is potentially more variable in papionins than previously thought. Since *Macaca* is widely acknowledged as representing the ancestral papionin morphotype (Delson 1975), another explanation would be that the absence of a lateral occipito-temporal sulcus corresponds to the ancestral condition. *Parapapio* would have retained this trait. This hypothesis would be in agreement with the previous findings that *Macaca* and *Parapapio* resemble one another in several ways (Szalay & Delson 1979; Beaudet *et al*. 2016b). Interestingly, the lateral positon of the occipito-temporal sulcus has been hypothesized to be the consequence of the caudo-lateral elongation of the inferior temporal gyrus which implies changes in visual capacities (Falk 1978). The development of visual capacities may have occurred after 5.37 Ma and be correlated with variation in the environment and food resources during the Plio-Pleistocene period (de Menocal 2004). Nonetheless, variation in the sulcal pattern of extinct and extant papionin endocasts needs to be further explored and coupled with the investigation of additional functional traits (e.g. cerebral asymmetries, Bouchet *et al*. 2017). Moreover, the application of functional imaging on such features would permit to test a potential relationship between endocranial variation and changes in the ecology of fossil primates. In a broader framework, it would be necessary to apply these analyses to a larger sample size.

We are indebted to the Evolutionary Studies Institute Fossil Access Advisory (Johannesburg) and L. Berger (Johannesburg) for having granted access to the U.W. 88-886 specimen; S. Potze (Pretoria), J. Cuisin (Paris) and G. Fleury (Toulouse) for access to comparative material. We also thank G. Clément and M. Garcia-Sanz (Paris) for microtomographic acquisitions at the MNHN; B. Duployer (Toulouse) at the CIRIMAT; F. de Beer (Pretoria) at Necsa. For scientific discussion we are grateful to J. Braga and J. Dumoncel (Toulouse). We thank S. Elton and F. L'Engle Williams for their comments as reviewers, which contributed to improving the original version of this manuscript. Costs of typesetting and digital archiving are borne by the Palaeontological Scientific Trust (PAST) and its Scatterlings of Africa Programmes, the DST/NRF Centre of Excellence in Palaeosciences, and the University of the Witwatersrand. Research supported by the Occitanie Region and the French Ministry of Higher Education and Research.

§ORCID iDs

J.L. Heaton: orcid.org/0000-0001-8039-4748
C. Tenailleau: orcid.org/0000-0001-5935-9745
B. Zipfel: orcid.org/0000-0002-4251-884X
A. Beaudet: orcid.org/0000-0002-9363-5966

REFERENCES

ALTMANN, S.A. 2009. Fallback foods, eclectic omnivores, and the packaging problem. *American Journal of Physical Anthropology*, **140**, 615–629.

BAMFORD, M.K., NEUMANN F.H., PEREIRA L.M., SCOTT L., DIRKS P.H.G.M. & BERGER L.R. 1999. Botanical remains from a coprolite from the Pleistocene hominin site of Malapa, Sterkfontein Valley, South Africa. *Palaeontologia africana*, **45**, 23–28.

BAYLE, P., BONDIOLI, L., MACCHIARELLI, R., MAZURIER, A., PUYMERAIL, L., VOLPATO, V. & ZANOLLI, C. 2011. Three-dimensional imaging and quantitative characterization of human fossil remains. Examples from the NESPOS database. **In:** Macchiarelli, R. & Weniger, G.C. (eds), *Pleistocene Databases. Acquisition, Storing, Sharing*, 29–49. Mettmann, Wissenschaftliche Schriften des Neanderthal Museums 4.

BEAUDET, A. 2015. Caractérisation des structures crânio-dentaires internes des cercopithécoïdes et étude diachronique de leurs variations morphologiques dans la séquence Plio-Pléistocène sud-africaine. Ph.D. thesis, Université de Toulouse, Toulouse.

BEAUDET, A., BRAGA, J., DE BEER, F., SCHILLINGER, B., STEININGER, C., VODOPIVEC, V. & ZANOLLI, C. 2016a. Neutron microtomography-based virtual extraction and analysis of a cercopithecoid partial cranium (STS 1039) embedded in a breccia fragment from Sterkfontein member 4 (South Africa). *American Journal of Physical Anthropology*, **159,** 737–745.

BEAUDET, A., DUMONCEL, J., THACKERAY, J.F., BRUXELLES, L., DUPLOYER, B., TENAILLEAU, C., BAM, L., HOFFMAN, J., DE BEER, F. & BRAGA, J. 2016b. Upper third molar internal structural organization and semicircular canal morphology in Plio-Pleistocene South African cercopithecoids. *Journal of Human Evolution*, **95,** 104–120.

BEAUDET, A., DUMONCEL, J., DE BEER, F., DUPLOYER, B., DURRLEMAN, S., GILISSEN, E., HOFFMAN, J., TENAILLEAU, C., THACKERAY, J.F. & BRAGA, J. 2016c. Morphoarchitectural variation in South African fossil cercopithecoid endocasts. *Journal of Human Evolution*, **101,** 65–78.

BERGER, L.R., DE RUITER, D.J., CHURCHILL, S.E., SCHMID, P., CARLSON, K.J., DIRKS, P.H.G.M. & KIBII, J.M. 2010. *Australopithecus sediba*: a new species of *Homo*-like australopith from South Africa. *Science*, **328,** 195–204.

BONDIOLI, L., BAYLE, P., DEAN, C., MAZURIER, A., PUYMERAIL, L., RUFF, C., STOCK, J.T., VOLPATO, V., ZANOLLI, C. & MACCHIARELLI, R. 2010. Technical note: morphometric maps of long bone shafts and dental roots for imaging topographic thickness variation. *American Journal of Physical Anthropology*, **142,** 328–334.

BOUCHET, F., RIBERON, A., DE BEER, F., GILISSEN, E., TENAILLEAU, C. & BEAUDET, A. 2017. A comparative study of endocranial shape asymmetries in extant and extinct cercopithecoid taxa. *Proceedings of the European Society for the Study of Human Evolution*, **6,** 29.

BRUNER, E. & SHERKAT, S. 2008. The middle meningeal artery: from clinics to fossils. *Child's Nervous System*, **24,** 1289–1298.

BRUXELLES, L., MAIRE, R., COUZENS, R., THACKERAY, F. & BRAGA, J. 2016. A revised stratigraphy of Kromdraai. **In**: Braga, J. & Thackeray, J.F. (eds), *Kromdraai. A Birthplace of* Paranthropus *in the Cradle of Humankind*, 49–68. Johannesburg, Sun Press.

BYRNE, R.W., WHITEN, A., HENZI, S.P. & McCULLOCH, F.M. 1993. Nutritional constraints on mountain baboons (*Papio ursinus*): implications for baboon socioecology. *Behavioral Ecology and Sociobiology*, **33,** 233–246.
CASTELLI, W.A. & HUELKE, D.F. 1965. The arterial supply of the dura mater of the rhesus monkey. *The Anatomical Record*, **152,** 155–160.
CODRON, D.M. 2003. Dietary ecology of chacma baboons (*Papio Ursinus* (Kerr, 1792)) and Pleistocene Cercopithecoidea in savanna environments of South Africa. Ph.D. thesis, University of Cape Town, Cape Town.
CONNOLLY, C.J. 1950. External morphology of the primate brain. Ph.D. thesis, Catholic University of America, Washington.
CONNOLLY, C.J. 1953. Brain morphology and taxonomy. *Anthropological Quarterly*, **26**(2), 35–65.
DAVENPORT, T.R.B., STANLEY, W.T., SARGIS, E.J., DE LUCA, D.W., MPUNGA, N.E., MACHAGA, S.J. & OLSON, L.E. 2006. A new genus of African monkey, *Rungwecebus*: morphology, ecology & molecular phylogenetics. *Science*, **312,** 1378–1381.
DE LAZARO G.R., EISOVA S., PISOVA H. & BRUNER E. 2018. The endocranial vascular system: tracing vessels. **In:** Bruner E., Ogihara N. & Tanabe H. (eds), *Digital Endocasts. Replacement of Neanderthals by Modern Humans Series*, 71–93. Tokyo, Springer.
DELSON, E. 1975. Evolutionary history of the Cercopithecidae. *Contributions to Primatology*, **4,** 167–217.
DELSON, E. 1984. Cercopithecid biochronology of the African Plio-Pleistocene: correlation among eastern and southern hominid-bearing localities. *Courier Forschungsinstitut Senckenberg*, **69,** 199–218.
DELSON, E. 1988. Chronology of South African australopith site units. **In:** Grine, F.E. (ed.), *Evolutionary History of the Robust Australopithecines*, 317–325. New York, Aldine de Gruyter.
DE MENOCAL, P.B. 2004. African climate change and faunal evolution during the Pliocene-Pleistocene. *Earth Planetary Science Letters*, **220,** 3–24.
DIRKS, P.H.G.M., KIBII, J.M., KUHN, B.F., STEININGER, C., CHURCHILL, S.E., KRAMERS, J.D., PICKERING, R., FARBER, D.L., MERIAUX, A.S., HERRIES, A.I.R., KING, G.C.P. & BERGER, L.R. 2010. Geological setting and age of *Australopithecus sediba* from southern Africa. *Science*, **328,** 205–208.
DUNBAR, R.I.M., & DUNBAR, E.P. 1974. Ecological relations and niche separation between sympatric terrestrial primates in Ethiopia. *Folia Primatologica*, **21,** 36–60.
DUNBAR, R.I.M. 1976. Australopithecine diet based on a baboon analogy. *Journal of Human Evolution*, **5,** 161–167.
EISENHART WL. 1974. The fossil cercopithecoids of Makapansgat and Sterkfontein. A.B. thesis, Harvard College, Cambridge.
ELTON, S. 2001. Locomotor and habitat classifications of cercopithecoid postcranial material from Sterkfontein Member 4, Bolt's Farm and Swartkrans Members 1 and 2, South Africa. *Palaeontologia africana*, **37,** 115–126.
ELTON, S. 2006. Forty years on and still going strong: the use of hominin–cercopithecid comparisons in palaeoanthropology. *Journal of the Royal Anthropological Institute*, **12,** 19–38.
ELTON, S. 2007. Environmental correlates of the cercopithecoid radiations. *Folia Primatologica*, **78,** 344–364.
ELTON, S. 2012. Impacts of environmental change and community ecology n the composition and diversity of the southern African monkey fauna from the Plio-Pleistocene to the present. **In:** Reynolds, S.C. & Gallagher, A. (eds), *African Genesis: Perspectives on Hominin Evolution*, 471–486. Cambridge, Cambridge University Press.
EL-ZAATARI, S., GRINE, F.E., TEAFORD, M.F. & SMITH, H.F. 2005. Molar microwear and dietary reconstructions of fossil cercopithecoidea from the Plio-Pleistocene deposits of South Africa. *Journal of Human Evolution*, **49,** 180–205.
FALK, D. 1978. Brain evolution in Old World Monkeys. *American Journal of Physical Anthropology*, **48,** 315–320.
FALK, D. 1981. Sulcal patterns of fossil *Theropithecus* baboons: phylogenetic and functional implications. *International Journal of Primatoly*, **2,** 57–69.
FALK, D. & NICHOLLS, P. 1992. Meningeal arteries in rhesus macaques (*Macaca mulatta*): implications for vascular evolution in anthropoids. *American Journal of Physical Anthropology*, **89,** 299–308.
FALK, D. 1993. Meningeal arterial patterns in great apes: implications for hominid vascular evolution. *American Journal of Physical Anthropology*, **92,** 81–97.
FASHING, P.J., NGUYEN, N., VENKATARAMAN, V.V. & KERBY, J.T. 2014. Gelada feeding ecology in an intact ecosystem at Guassa, Ethiopia: variability over time and implications for theropith and hominin dietary evolution. *American Journal of Physical Anthropology*, **155,** 1–16.
FLEAGLE, J.G. 2013. *Primate Adaptation and Evolution* (3rd edn). New York, Academic Press.
FREEDMAN, L. 1957. The fossil cercopithecoidea of South Africa. *Annals of the Transvaal Museum*, **23,**123–262.
FREEDMAN, L. 1961. New cercopithecoid fossils, including a new species, from Taung, Cape Province, South Africa. *Annals of the South African Museum*. **46**(1), 1–19.
FROST, S.R. 2007. Fossil cercopithecidae from the Middle Pleistocene Dawaitoli formation, Middle Awash valley, Afar region, Ethiopia. *American Journal of Physical Anthropology*, **134,** 460–471.
FROST, S.R. & ALEMSEGED, Z. 2007. Middle Pleistocene fossil Cercopithecidae from Asbole, Afar Region, Ethiopia. *Journal of Human Evolution*, **53,** 227–259.
FROST, S.R., ROSENBERGER, A.L. & HARTWIG, W.C. 2011. Old World Monkeys. **In:** John Wiley & Sons, Ltd (eds), *Encyclopedia of Life Sciences*, 1–6. Chichester, U.K., John Wiley & Sons.
GILBERT, C.C. 2007. Craniomandibular morphology supporting the diphyletic origin of mangabeys and a new genus of the *Cercocebus/Mandrillus* clade, *Procercocebus*. *Journal of Human Evolution*, **53,** 69–102.
GILBERT, C.C. & ROSSIE, J.B. 2007. Congruence of molecules and morphology using a narrow allometric approach. *Proceedings of the National Academy of Sciences*, **104,** 11910–11914.
GILBERT, C.C., FROST, S.R. & STRAIT, D.S. 2009. Allometry, sexual dimorphism & phylogeny: a cladistic analysis of extant African papionins using craniodental data. *Journal of Human Evolution*, **57**, 298–320.
GILBERT, C.C., STANLEY, W.T., OLSON, L.E., DAVENPORT, T.R.B. & SARGIS, E.J. 2011. Morphological systematics of the kipunji (*Rungwecebus kipunji*) and the ontogenetic development of phylogenetically informative characters in the Papionini. *Journal of Human Evolution*, **60,** 731–745.
GILBERT, C.C. 2013. Cladistic analysis of extant and fossil African papionins using craniodental data. *Journal of Human Evolution*, **64,** 399–433.
GILBERT, C.C., FROST, S.R., DELSON, E. 2013. Appearance of the modern baboon, *Papio hamadryas*, in the Plio-Pleistocene fossil record: evidence from South Africa. *American Journal of Physical Anthropology*, S56, **150,** 129.
GILBERT, C.C., STEININGER, C.M., KIBII, J.M. & BERGER, L.R. 2015. *Papio* cranium from the hominin-bearing site of Malapa: implications for the evolution of modern baboon cranial morphology and South African Plio-Pleistocene biochronology. *PLOS ONE*, 10, e0133361.
GILBERT, C.C., FROST, S.R., PUGH, K.D., ANDERSON, M. & DELSON, E. 2018. Evolution of the modern baboon (*Papio hamadryas*): a reassessment of the African Plio-Pleistocene record. *Journal of Human Evolution.* https://doi.org/10.1016/j.jhevol.2018.04.012
GÓMEZ-ROBLES, A., SMAERS, J.B., HOLLOWAY, R.L., POLLY, P.D. & WOOD, B.A. 2017. Brain enlargement and dental reduction were not linked in hominin evolution. *Proceedings of the National Academy of Sciences*, **114**(3), 468–473.
GOMMERY, D., SÉNÉGAS, F., KGASI, L., VILAKAZI, N., KUHN, B., BRINK, J., PICKFORD, M., HERRIES, A.I.R., HANCOX, J., SAOS, T., SÉGALEN, L., AUFORT, J. & THACKERAY, J.F. 2016. Bolt's Farm Cave System dans le Cradle of Humankind (Afrique du Sud): un exemple d'approche multidisciplinaire dans l'étude des sites à primates fossiles. *Revue de Primatologie*, **7**. http://journals.openedition.org/primatologie/2725
GONZALES, L.A., BENEFIT, B.R., McCROSSIN, M.L. & SPOOR, F. 2015. Cerebral complexity preceded enlarged brain size and reduced olfactory bulbs in Old World monkeys. *Nature Communications*, **6**(7580), 1–9.
HAMILTON, W.J., BUSKIRK, R.E. & BUSKIRK, W.H. 1978. Omnivory and utilization of food resources by chacma baboons, *Papio ursinus*. *The American Naturalist*, **112,** 911–924.
HARTSTONE-ROSE, A., KUHN, B.F., NALLA, S., WERDELIN, L. & BERGER, L.R. 2013. A new species of fox from the *Australopithecus sediba* type locality, Malapa, South Africa. *Transaction of the Royal Society of South Africa*, **68,** 1–9.
HEATON, J.L. 2006. Taxonomy of the Sterkfontein fossil Cercopithecinae: the Papionini of members 2 and 4 (Gauteng, South Africa). Ph.D. thesis, Indiana University, Bloomington.
HERRIES, A.I.R., CURNOE, D. & ADAMS, J.W. 2009. A multi-disciplinary seriation of early *Homo* and *Paranthropus* bearing palaeocaves in southern Africa. *Quaternary International*, **202,** 14–28.
HOFFMAN, J.W., DE BEER, F.C. 2012. Characteristics of the micro-focus X-ray tomography facility (MIXRAD) at Necsa in South Africa. *Proceedings of the 18th World Conference of Nondestructive Testing*, Durban, South Africa.
JABLONSKI, N.G. 2002. Fossil Old World monkeys: the late Neogene radiation. **In:** Hartwig, W. (ed.), *The Primate Fossil Record*, 255–299. Cambridge, Cambridge University Press.
JABLONSKI, N.G. & FROST, S. 2010. Cercopithecoidea. **In:** Werdelin, L. & Sanders, W. (eds), *Cenozoic Mammals of Africa*, 383–428. Berkeley, University of California Press.

JARVEY, J.C., LOW, B.S., PAPPANO, D.J., BERGMAN, T.J. & BEEHNER, J.C. 2018. Graminivory and fallback foods: annual diet profile of geladas (*Theropithecus gelada*) living in the Simien Mountains National Park, Ethiopia. *International Journal of Primatology*, **39,** 105–126.
KONO, R.T. 2004. Molar enamel thickness and distribution patterns in extant great apes and humans: new insights based on a 3-dimensional whole crown perspective. *Anthropological Science*, **112,** 121–146.
KOVACS, I. 1979. The surface characteristics of tooth roots and their biomechanical importance. *International Journal of Skeletal Research*, **6,** 181–192.
KUHN, B.F., WERDELIN, L., HARTSTONE-ROSE, A., LACRUZ, R.S. & BERGER, L.R. 2011. Carnivoran remains from the Malapa hominin site, South Africa. *PLOS ONE*, **6**, e26940.
KUPCZIK, K. & DEAN, M.C. 2008. Comparative observations on the tooth root morphology of *Gigantopithecus blacki*. *Journal of Human Evolution*, **54,** 196–204.
KUPCZIK, K., OLEJNICZAK, A.J., SKINNER, M.M., HUBLIN, J.-J. 2009. Molar crown and root size relationship in anthropoid primates. Frontiers of Oral Biology Series, 13. **In:** Koppe, T., Meyer, G. & Alt, K.W. (eds), *Comparative Dental Morphology*, 16–22. Basel, Karger.
KUPCZIK, K. & HUBLIN, J.-J. 2010. Mandibular molar root morphology in Neanderthals and Late Pleistocene and recent *Homo sapiens*. *Journal of Human Evolution*, **59,** 525–541.
LE CABEC, A., KUPCZIK, K., GUNZ, P., BRAGA, J. & HUBLIN, J.-J. 2012. Long anterior mandibular tooth roots in Neanderthals are not the result of their large jaws. *Journal of Human Evolution*, **63,** 667–681.
LE CABEC, A., GUNZ, P., KUPCZIK, K., BRAGA, J. & HUBLIN, J.-J. 2013. Anterior tooth root morphology and size in Neanderthals: taxonomic and functional implications. *Journal of Human Evolution*, **64,** 169–193.
MACCHIARELLI, R., BAYLE, P., BONDIOLI, L., MAZURIER, A. & ZANOLLI, C. 2013. From outer to inner structural morphology in dental anthropology: integration of the third dimension in the visualization and quantitative analysis of fossil remains. **In:** Scott., G.R. & Irish, J.D. (eds), *Anthropological Perspectives on Tooth Morphology: Genetics, Evolution, Variation*, 250–277. Cambridge, Cambridge University Press.
MAIER, W. 1972. The first complete skull of *Simopithecus darti* from Makapansgat, South Africa & its systematic position. *Journal of Human Evolution*, **1,** 395–405.
MARSHALL, A.J. & WRANGHAM, R.W. 2007. Evolutionary consequences of fallback foods. *International Journal of Primatology*, **28,** 1219–1235.
MARSHALL, A.J., BOYKO, C.M., FEILEN, K.L., BOYKO, R.H. & LEIGHTON, M. 2009. Defining fallback foods and assessing their importance in primate ecology and evolution. *American Journal of Physical Anthropology*, **140,** 603–614.
McGRAW, W.S., VICK, A.E. & DAEGLING, D.J. 2014. Dietary variation and food hardness in sooty mangabeys (*Cercocebus atys*): implications for fallback foods and dental adaptation. *American Journal of Physical Anthropology*, **154,** 413–423.
NEWMAN, T.K., JOLLY, C.J. & ROGERS, J. 2004. Mitochondrial phylogeny and systematics of baboons (*Papio*). *American Journal of Physical Anthropology*, **124,** 17–27.
OLEJNICZAK, A.J., SMITH, T.M., FEENEY, R.N.M., MACCHIARELLI, R., MAZURIER, A., BONDIOLI, L., ROSAS, A., FORTEA, J., DE LA RASILLA, M., GARCIA-TABERNERO, A., RADOVČIĆ, J., SKINNER, M.M., TOUSSAINT, M. & HUBLIN, J.-J. 2008a. Dental tissue proportions and enamel thickness in Neandertal and modern human molars. *Journal of Human Evolution*, **55,** 12–23.
OLEJNICZAK, A.J., TAFFOREAU, P., FEENEY, R.N.M. & MARTIN, L.B. 2008b. Three-dimensional primate molar enamel thickness. *Journal of Human Evolution*, **54,** 187–195.
PERELMAN, P., JOHNSON, W.E., ROOS, C., SEUÁNEZ, H.N., HORVATH, J.E., MOREIRA, M.A.M., KESSING, B., PONTIUS, J., ROELKE, M., RUMPLER, Y., SCHNEIDER, M.P.C., SILVA, A., O'BRIEN, S.J. & PECON-SLATTERY, J. 2011. A molecular phylogeny of living primates. *PLOS Genetics*, 7, e1001342.
PICKFORD, M. 2013. The diversity, age, biogeographic and phylogenetic relationships of Plio-Pleistocene suids from Kromdraai, South Africa. *Annals of the Ditsong National Museum of Natural Hististory*, **3,** 11–32.
PUGH, K.D. & GILBERT, C.C. 2018. Phylogenetic relationships of living and fossil African papionins: combined evidence from morphology and molecules. *Journal of Human Evolution*, https://doi.org/10.1016/j.jhevol.2018.06.002
RADINSKY, L. 2005. The fossil evidence of anthropoid brain evolution. *American Journal of Physical Anthropology*, **41,** 15–27.
REED, K.E. 1996. Early hominid evolution and ecological change through the African Plio-Pleistocene. *Journal of Human Evolution*, **32,** 289–322.
SINGLETON, M., McNULTY, K.P., FROST, S.R., SODERBERG, J. & GUTHRIE, E.H. 2010. Bringing up baby: developmental simulation of the adult cranial morphology of *Rungwecebus kipunji*. *The Anatomical Record: Advances in Integrative Anatomy and Evolutionary Biology*, **293,** 388–401.
SPENCER, M.A. 1998. Force production in the primate masticatory system: electromyographic tests of biomechanical hypotheses. *Journal of Human Evolution*, **34,** 25–54.
SPENCER, M.A. 2003. Tooth-root form and function in platyrrhine seed-eaters. *American Journal of Physical Anthropology*, **122,** 325–335.
STEININGER, C., BERGER, L.R. & KUHN, B.F. 2008. A partial skull of *Paranthropus robustus* from Cooper's Cave, South Africa. *South African Journal of Science*, **104,** 143–146.
SZALAY, F.S. & DELSON, E. 1979. *Evolutionary History of the Primates*. Academic Press, New York.
VAL, A., DIRKS, P.H.G.M., BACKWELL, L.R., D'ERRICO, F. & BERGER, L.R. 2015. Taphonomic analysis of the faunal assemblage associated with the hominins (*Australopithecus sediba*) from the Early Pleistocene cave ceposits of Malapa, South Africa. *PLOS ONE*, 10, e0126904.
VENKATARAMAN, V.V., GLOWACKA, H., FRITZ, J., CLAUSS, M., SEYOUM, C., NGUYEN, N. & FASHING, P. J. 2014. Effects of dietary fracture toughness and dental wear on chewing efficiency in geladas (*Theropithecus gelada*). *American Journal of Physical Anthropology*, **155,** 17–32.
VRBA, E.S. 1975. Some evidence of chronology and palaeoecology of Sterkfontein, Swartkrans and Kromdraai from the fossil Bovidae. *Nature*, **254,** 301–304.
WILLIAMS, F.L., ACKERMANN, R.R. & LEIGH, S.R. 2007. Inferring Plio-Pleistocene southern African biochronology from facial affinities in *Parapapio* and other fossil papionins. *American Journal of Physical Anthropology*, **132,** 163–174.
WILLIAMS, B.A., ROSS, C.F., FROST, S.R., WADDLE, D.M., GABA-DIRWE, M. & BROOK, G.A. 2012. Fossil *Papio* cranium from?!Ncumtsa (Koanaka) Hills, western Ngamiland, Botswana. *American Journal of Physical Anthropology*, **149,** 1–17.
ZANOLLI, C., BONDIOLI, L., COPPA, A., DEAN, C.M., BAYLE, P., CANDILIO, F., CAPUANI, S., DREOSSI, D., FIORE, I., FRAYER, D.W., LIBSEKAL, Y., MANCINI, L., ROOK, L., MEDIN TEKLE, T., TUNIZ, C. & MACCHIARELLI, R. 2014. The late Early Pleistocene human dental remains from Uadi Aalad and Mulhuli-Amo (Buia), Eritrean Danakil: macromorphology and microstructure. *Journal of Human Evolution*, **74,** 96–113.
ZANOLLI, C., PAN, L., DUMONCEL, J., KULLMER, O., KUNDRÁT, M., LIU, W., MACCHIARELLI, R., MANCINI, L., SCHRENK, F. & TUNIZ, C. 2018. Inner tooth morphology of *Homo erectus* from Zhoukoudian. New evidence from an old collection housed at Uppsala University, Sweden. *Journal of Human Evolution*, **116,** 1–13.
ZINNER, D., ARNOLD, M.L. & ROOS, C. 2009. Is the new primate genus *Rungwecebus* a baboon? *PLOS ONE*, 4, e4859.